Available online at www.sciencedirect.com
SCIENCE DIRECT®
PERGAMON
Scripta Materialia 48 (2003) 949–954
Scripta MATERIALIA
www.actamat-journals.com

Magnetic reversal of ion beam patterned Co/Pt multilayers

Greg J. Kusinski [a,b,c,*], Kannan M. Krishnan [c,d], Gregory Denbeaux [c], Gareth Thomas [a,b,c]

[a] *MMFX Technologies, R&D, 2 Corporate Park Suite 102 R&D, Irvine, CA 92606, USA*
[b] *Department of Materials Science and Engineering, University of California, Berkeley, CA 94720, USA*
[c] *Materials Sciences Division, Lawrence Berkeley National Laboratory, Berkeley, CA 94720, USA*
[d] *Department of Materials Science and Engineering, University of Washington, Seattle, WA 98195, USA*

Received 1 August 2002; received in revised form 24 September 2002; accepted 25 September 2002

Abstract

The characteristics of the reversal processes of magnetic arrays fabricated by ion-irradiation of Co/Pt multilayers with perpendicular magnetic anisotropy are reported. Magnetic patterns with periodicities from 1 μm to 100 nm were patterned. A correlation between the pattern size, magnetic reversal and grain size is presented.

Keywords: Multilayers; Magnetic imaging; Magnetic domains; Transmission X-ray microscopy; Transmission electron microscopy

1. Introduction and background

In order to sustain the growth of magnetic recording, the limitations associated with superparamagnetic grains must be solved [1]. The new approach to ultrahigh-density magnetic storage, is based on patterning of perpendicular magnetic media into individual single domain elements [2]. A specific example is the Co/Pt multilayer (ML) structure with perpendicular magnetic anisotropy (PMA), where the PMA can be systematically reduced by ion irradiation [3–5].

In this paper the characteristics of the reversal processes of magnetic arrays fabricated by ion-irradiation of Co/Pt multilayers (MLs) are reported. The MLs {20 nm Pt seed/10 (0.3 nm Co/1 nm Pt)/1 nm Pt cap layer} with perpendicular anisotropy were deposited by electron beam evaporation onto electron transparent Si_3N_4 windows. Previously the effects of growth temperature and ion-irradiation on the microstructure and the magnetic domain structure were investigated [5–8]. It is known that with an increasing dose of ion irradiation the perpendicular coercivity H_C of the Co/Pt MLs decreases without affecting the square loop shape. With further increase in the irradiation dose, the transition from out-of-plane to in-plane easy magnetization axis is obtained. This ability to control and vary the magnetic property by ion-irradiation, makes Co/Pt MLs very attractive for patterned media applications [9–11].

* Corresponding author. Present address: MMFX Technologies, R&D, 2 Corporate Park Suite 102 R&D, Irvine, CA 92606, USA. Tel.: +1-9494767600; fax: +1-9494741130.
E-mail address: kusinski@calalum.org (G.J. Kusinski).

1359-6462/03/$ - see front matter © 2003 Acta Materialia Inc. Published by Elsevier Science Ltd. All rights reserved.
doi:10.1016/S1359-6462(02)00607-3

Using the principles of ion-irradiation, two techniques to locally modify the magnetic properties of the Co/Pt multilayers were applied. In the first patterning method, a uniform intensity large beam of 700 keV N^+ ions was used to irradiate the samples through a Si stencil mask with 1.4 μm regularly spaced circular holes [10]. In the second patterning approach, a 30 keV Ga^+ focused ion beam (FIB), with 20 nm beam size was used to directly "write" features on the sample.

The magnetic transmission X-ray microscopy (MTXM), which is sensitive to out-of-plane magnetization [12], was utilized to study the reversals of samples with perpendicular anisotropy. The samples were imaged at 25 nm resolution with the full field soft X-ray transmission microscope located at the Beamline 6.1.2 of the Advanced Light Source at Lawrence Berkeley National Laboratory [12]. In this technique the magnetic contrast is based on the absorption of photons, a process governed by electronic dipole transitions known as X-ray magnetic circular dichroism. The basic principles of contrast formation are shown in Fig. 1. The parallel (anti-parallel) alignment of the positive (negative) magnetization and polarization results in increased (decreased) absorption of photons at the Co L_3 edge, seen as dark (bright) areas in the image [13].

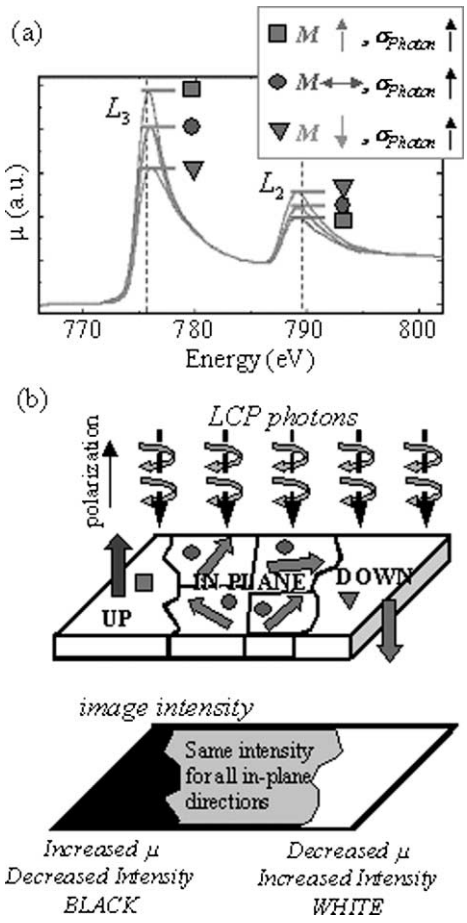

Fig. 1. Schematic diagrams illustrating the magnetic contrast mechanism in the MTXM: (a) L_3 and L_2 absorption edges with three levels of absorption coefficient (μ) depending on the relative orientation of magnetization (M) and photon polarization (σ_{photon}); (b) magnetic sample with up, down and in-plane domains and a recorded image displaying three intensity levels.

2. Results and discussion

For comparison, various patterns imaged with MTXM are displayed at the same magnification in Fig. 2. The images show:

- Fig. 2(a) 6×6 μm^2 image, 1.3 μm circular regions were patterned by irradiation through the stencil mask with 700 keV 5×10^{16} N^+/cm^2 and have in-plane magnetization. The image was recorded after saturation at -14 kOe (white regions) and reversal to $+4$ kOe (nucleation black regions). The in-plane magnetization of the irradiated regions was also confirmed by Lorentz transmission electron microscopy (LTEM) [14], which is sensitive to in-plane magnetization [15]. Fig. 2(b) shows Fresnel LTEM image recorded at 500 Oe in-plane field, which was sufficient to saturate the irradiated regions.
- Fig. 2(c) a FIB pattern with 140 nm in-plane lines defining 310 nm squares with PMA. The image was recorded after saturation at -14 kOe (white regions) and reversal to $+3$ kOe (black regions). The black contrast at the squares' edges indicates softening as compared to the matrix. Again note that the "black" reversal started at the pattern boundaries.
- Fig. 2(d) a FIB pattern with 100 nm in-plane squares, image recorded after demagnetization.

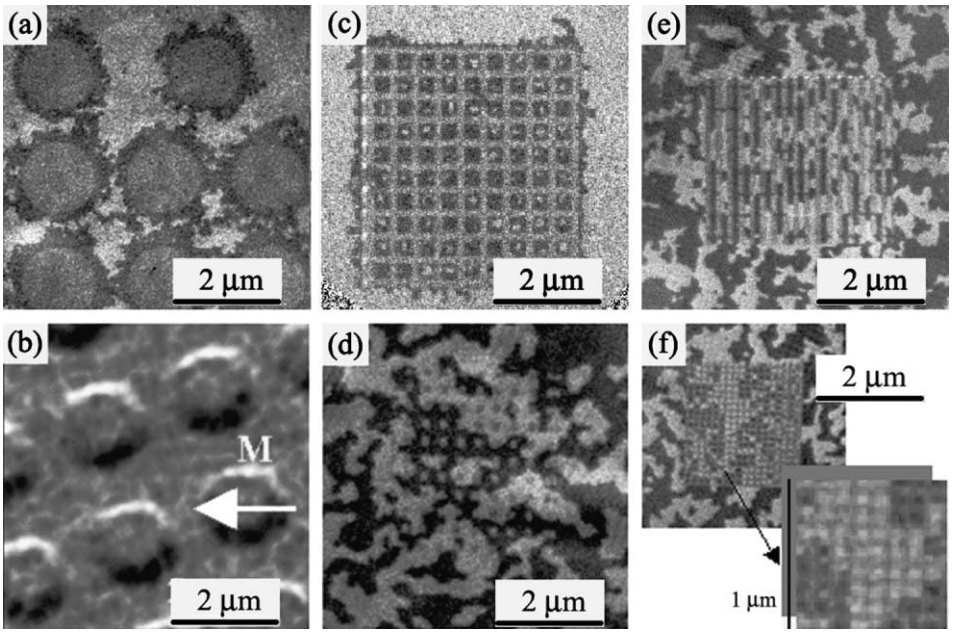

Fig. 2. MTXM images of ion-irradiation patterned Co/Pt MLs. All images are displayed at same magnification, except for insert in (f), see text.

- Fig. 2(e) a FIB pattern with 80×320 nm^2 in-plane rectangles, image recorded after demagnetization. Sharp transitions between in-plane (gray) and out-of-plane (black or white) regions indicate high resolution of the pattering technique.
- Fig. 2(f) a FIB pattern with 40 nm in-plane lines defining 100 nm squares with PMA, insert shows a 1 μm area.

As shown a variety of patterns can be created with feature sizes below 40 nm. Referring back to the microstructural characterization [6], the grain size in the discussed multilayers was approximately 50–100 nm. Pattering across individual grains was obtained in all cases as the roughness of the pattern boundaries is below that of the microstructure, indicating that the ion-irradiation patterning technique is microstructure independent. For all presented patterns, the X-ray absorption images recorded with photons away from the Co absorption edge had uniform contrast (images not shown). This proves that the patterned samples have uniform thickness and the contrast presented in Fig. 2 is only magnetic without any topographic contribution.

Below, the reversal processes of patterned Co/Pt multilayers are discussed based on the stencil mask pattern shown in Fig. 2(a). Fig. 3 shows a MTXM image recorded at remanence after saturation with $H_\perp = -14$ kOe and subsequent application of $H_\perp = +5$ kOe. The dark contrast corresponds to perpendicular up, positive magnetization, bright contrast to perpendicular down, negative magnetization, and gray contrast (average intensity) to in-plane magnetization in accordance with Fig. 1. The initial stages of nucleation of positive domains were recorded near the edges of the irradiated patterns at fields as low as $H_\perp \leqslant +1$ kOe, which were well below the nucleation field of the as-grown film ($H^\circ_{N\perp} \cong 4.5$ kOe). Only after application of $H_\perp$ between +4 and +5 kOe, the nucleation of the reversed black domains away from the edge of the irradiated pattern was first observed, note the isolated boot shaped domain in Fig. 3. This suggests that ion irradiation introduces low-field nucleation centers at the irradiation pattern boundaries. Similar effects were observed by Ferre et al. [4].

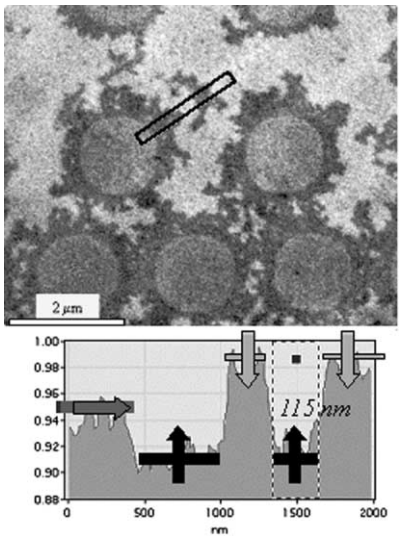

Fig. 3. MTXM image of patterned Co/Pt MLs and a normalized line profile obtained from the area labeled with the rectangle.

As shown in Figs. 2 and 3 the roughness of the reversal domains is suggestive of microstructure-governed perpendicular reversal. Two images of the same sample location collected after (1) saturation with $H_\perp = -14$ kOe followed by application of a reversed field $H_\perp = +4$ kOe, and (2) saturation with $H_\perp = +14$ kOe and application of $H_\perp = -4$ kOe, are shown in Fig. 4. These images show exactly complementary contrast. The extent of the reversed domains, black areas in Fig. 4(a) and white areas in Fig. 4(b), is identical. The reversed domains are pinned in exactly the same locations, indicating a return point memory. The magnetic reversal in these Co/Pt MLs is not random but is governed by the underlying physical microstructure and interactions at mask interfaces. Indeed, the length scale associated with the roughness of the reversed domains is comparable with the physical dimensions of the columnar grains reported in [6]. The microstructure and, in particular, the columnar grain size influences the domain-wall pinning and the reversal processes [8], consistent with theoretical modeling of Lemerle et al. for Pt/Co/Pt sandwich-like structures [16].

Fig. 5 shows an image recorded at remanence after the following magnetizing sequence: (1) saturation with $H_\perp = +14$ kOe then (2) application of $H_\perp = -5$ kOe followed by (3) application of $H_\perp = +3$ kOe. As shown, a double ring of reversed white and black domains around the irradiation patterns was recorded. The progress of this magnetic process is illustrated schematically in the same figure. After the first step, the matrix was uniformly magnetized up as shown by the black contrast. When -5 kOe was applied, step 2, down—white domains nucleated at the patterns boundaries and propagated outwards, approximately 350 nm into the matrix. When the field was reversed again, but only to $+3$ kOe (step 3), new up—black domains were nucleated at the pattern boundaries. These black domains propagated outwards and partially consumed the previously nucleated white domains. However, the new black domains extend only up to approximately 180 nm away from the boundary. This magnetizing experiment confirms that the nucleation of reversed domains always starts at the pattern boundaries,

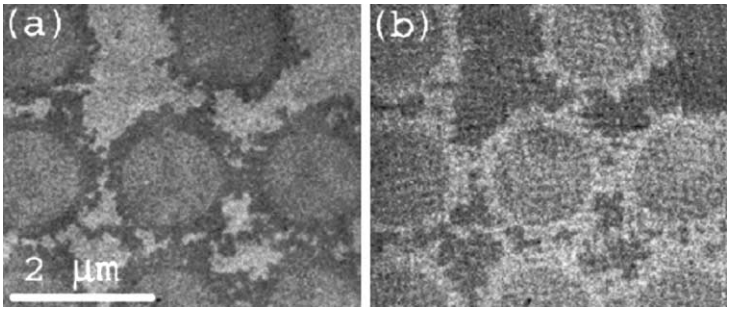

Fig. 4. MTXM images of same sample location imaged after (a) $H_\perp = -14$ kOe and $H_\perp = +4$ kOe (b) $H_\perp = +14$ kOe and $H_\perp = -4$ kOe.

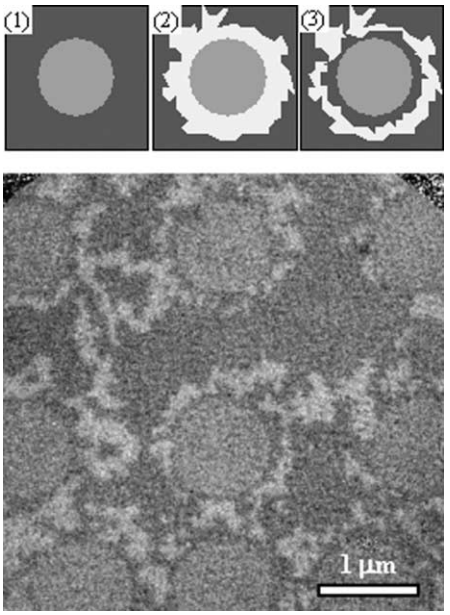

Fig. 5. MTXM image recorded at remanence after the following magnetizing sequence: (1) saturation with $H_{\perp} = +14$ kOe, (2) application of $H_{\perp} = -5$ kOe, (3) application of $H_{\perp} = +3$ kOe. Schematics show the domain evolution during these three magnetizing steps.

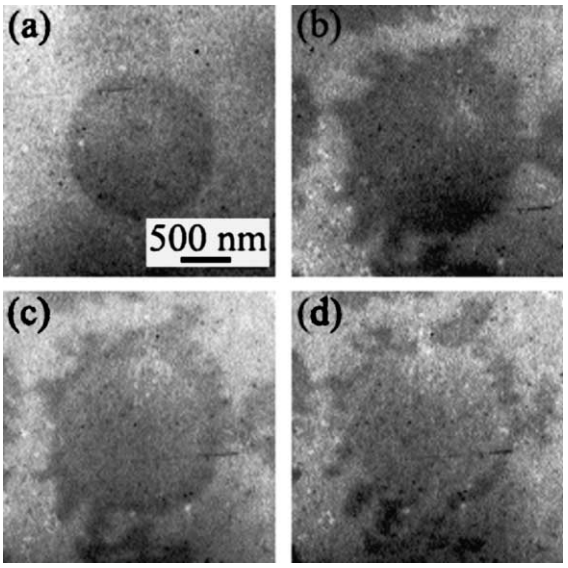

Fig. 6. Progress of the in situ magnetizing experiment. Images were acquired with the magnetic field on. Unfortunately due to experimental difficulties, the incident photon intensity is not uniform across the images. The reader is asked to compare only the relative local intensities on each image, and not the overall intensity, nor intensities between images directly: (a) $H_{\perp} = 0$ kOe, (b) $H_{\perp} = +3$ kOe, (c) $H_{\perp} = 0$ kOe and (d) $H_{\perp} = -1$ kOe.

as shown by the double rings of black and white domains, and proceeds outwards. What, however, is very important to note from Fig. 5 is that after step 3, the domain walls between the original black matrix and the white domains are pinned at the same location as they were after step 2, (i.e. ~350 nm). The pinning strength at that location is higher than the field applied during step 3, which was 3 kOe. This shows that both H_C and H_P increase gradually from the lowest value at the irradiation boundaries up to the original values of the as-grown samples at some distance away from the boundary.

To further elucidate the information about details of the reversal process, *IN-SITU* magnetizing experiments were conducted, Fig. 6. Before starting, the sample was saturated with -14 kOe field. When imaged at remanence, the sample had a uniform light—down magnetized matrix and a darker, gray irradiated disk indicating in-plane magnetization. When $H_{\perp} = +3$ kOe was applied, rotation of the magnetization in the irradiated regions and reversal of the adjacent areas was observed, Fig. 6(b). Two levels of photon absorption were measured, black-reversed and white, corresponding to up and down domains, respectively. When the perpendicular field was turned off and an image recorded at remanence, three levels of photon intensity were measured, Fig. 6(c). The magnetization in the ion-irradiated regions collapsed to in-plane, which is seen as an intermediate contrast. Note that this intermediate gray level corresponding to in-plane domains was not present in Fig. 6(b). When $H_{\perp} = -1$ kOe was applied, Fig. 6(d), the irradiated regions, and to small extend some adjacent regions, switch to down, white, magnetization. Note that the intermediate gray level corresponding to in-plane domains is gone.

The sequence shows that the reversal process is not precisely associated with the irradiation boundary alone. The reversal starts by rotation of the in-plane regions and subsequent propagation of magnetic domains into the perpendicular matrix. Fig. 7 schematically illustrates this process. As increasingly larger reverse fields are applied the

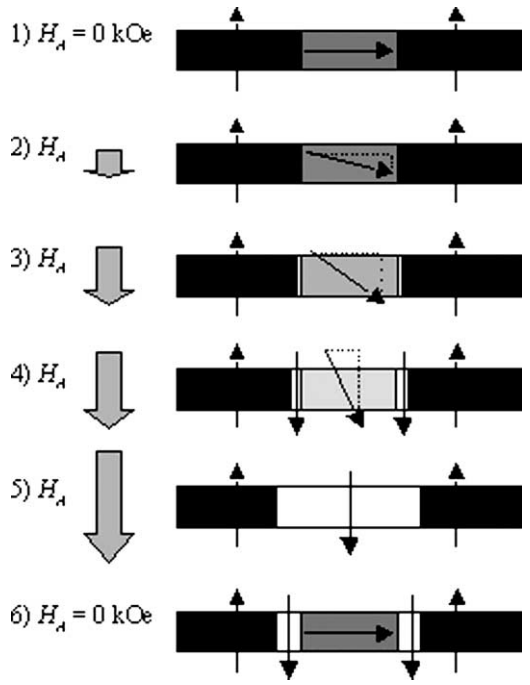

Fig. 7. Schematic of the reversal process. Sample colors indicate the orientation of magnetization.

magnetization of the irradiated regions is rotated and at some point, step 3 in the schematic, the down magnetization extends into the non-irradiated matrix. With further increase in the downward field, both the rotation of the in-plane magnetization continues and the grown of the down domains occurs. At a certain field, as show in step 5, the irradiated regions are completely rotated and have the same contrast as the reversed down regions. When the field is removed, the irradiated regions collapse back to in-plane, but the newly reversed down regions remain, as shown in step 6.

3. Summary

The boundaries of the patterns, defined by the transition from out-of-plane to in-plane magnetization, were found to be determined by the mask, while the scale of the magnetic reversal was governed by the microstructure. The main characteristic of perpendicular reversal in such ion-beam patterned MLs is the presence of the low-field nucleation centers at the irradiation pattern boundaries. Magnetic reversal always starts at the pattern boundaries; followed by domain wall motion into the non-irradiated region. *IN-SITU* data showed that the perpendicular reversal process starts by rotation of the in-plane regions, followed by propagation into the matrix.

Acknowledgements

Work at NCEM/LBNL was supported by the US Department of Energy under contract no. DE-AC03-76SF00098. G.K. acknowledges financial support through the "IBM Research Fellowship". The authors acknowledge contributions from E.C. Nelson, B.D. Terris, C.T. Rettner, A. Kellock and J.E.E. Bagglin.

References

[1] White RL. J Magn Magn Mater 2000;209:1.
[2] Ross C. Ann Rev Mater Res 2001;31:203.
[3] Chappert C, Bernas H, Ferre J, Kottler V, Jamet J-P, Chen Y, et al. Science 1998;280:1919.
[4] Ferre J, Chappert C, Bernas H, Jamet J-P, Meyer P, Kaitasov O, et al. J Magn Magn Mater 1999;191:198.
[5] Weller D, Baglin JEE, Kellock AJ, Hannibal KA, Toney MF, Kusinski GJ, et al. J Appl Phys 2000;87:5768.
[6] Kusinski GJ, Thomas G, Denbeaux G, Krishnan KM, Terris BD. J Appl Phys 2002;91:7541.
[7] Kusinski GJ, Thomas G. Microsc Microanal 2002;8:319.
[8] Weller D, Folks L, Best M, Fullerton EE, Terris BD, Kusinski GJ, et al. J Appl Phys 2001;89:7525.
[9] Devolder T, Chappert C, Chen Y, Cambril E, Bernas H, Jamet JP, et al. Appl Phys Lett 1999;74:3383.
[10] Terris BD, Folks L, Weller D, Baglin JEE, Kellock AJ, Rothuizen H, et al. Appl Phys Lett 1999;75:403.
[11] Kusinski GJ, Krishnan KM, Denbeaux G, Thomas G, Weller D, Terris BD. Appl Phys Lett 2001;79:2211.
[12] Denbeaux G, Fischer P, Kusinski G, Gros ML, Pearson A, Attwood D. IEEE Trans Magn 2001;37:2764.
[13] Stohr J, Padmore HA, Anders S, Stammler T, Scheinfein MR. Surf Rev Lett 1998;5:1297.
[14] Kusinski GJ, Krishnan KM, Weller D, Terris BD, Folks L, Kellock AJ, et al. Magnetic storage systems beyond 2000. New York: Kluwer Academic Publishers; 2001. p. 157.
[15] Chapman JN, Scheinfein MR. J Magn Magn Mater 1999;200:729.
[16] Lemerle S, Ferre J, Chappert C, Mathet V, Giamarchi T, LeDoussal P. Phys Rev Lett 1998;80:849.